Materials Research. 2018; 21(6): e20171004
DOI: http://dx.doi.org/10.1590/1980-5373-MR-2017-1004

Layered Double Hydroxides as Hosting Matrices for Storage and Slow Release of Phosphate Analyzed by Stirred-Flow Method

Luíz Paulo Figueredo Benício[a]*, Denise Eulálio[a], Luciano de Moura Guimarães[b], Frederico Garcia Pinto[a], Liovando Marciano da Costa[c], Jairo Tronto[a]

[a]Instituto de Ciências Exatas e Tecnológicas, Universidade Federal de Viçosa, Campus de Rio Paranaíba, Rodovia MG-230, km 07, 38810-000, Rio Paranaíba, MG, Brasil
[b]Departamento de Física, Universidade Federal de Viçosa, Avenida Peter Henry Rolfs, 36570-000, Viçosa, MG, Brasil
[c]Departamento de Solos, Universidade Federal de Viçosa, Avenida Peter Henry Rolfs, Edifício Silvyo Starling Brandão, 36570-000, Viçosa, MG, Brasil

Received: November 11, 2017; Revised: July 05, 2018; Accepted: August 05, 2018

The objective of this work was to synthesize and characterize Layered Double Hydroxides (MgAl-LDHs, MgFe-LDHs, and MgAlFe-LDHs) containing phosphate anions and study P release kinetics was conducted with the prepared materials. The release kinetics tests were performed in water by the stirred-flow method to verify the P release profile from LDHs materials. Results showed LDHs have similar characteristics to those of reactive sources of P, such as thermophosphates. The LDHs presented gradual P release and the LDH prepared with the molar ratio of cations Mg:Al = 2:1 showed a more sustained profile of P release compared to other produced materials. Thus, the chemical and structural characteristics of the LDHs make them potential materials for the use and storage of slow P release fertilizer.

Keywords: *fertilizers, nanotechnology, P kinetic release, stirred-flow method.*

1. Introduction

Layered Double Hydroxides (LDHs), also known as hydrotalcite like compounds, are materials with a bidimensional (2D) structure[1]. LDHs can be represented by the chemical formula $[M^{2+}_{(1-x)}M^{3+}_{x}(OH)_2](A^{n-})_{x/n}\cdot zH_2O$, where M^{2+} refers to bivalent metallic cations, such as Mg^{2+}, Cr^{2+}, Ca^{2+}, Fe^{2+}, Mn^{2+}, Co^{2+}; M^{3+} refers to trivalent metallic cations, such as Al^{3+}, Co^{3+}, Fe^{3+}, Cr^{3+}, and A^{n-} refers to interlayer anions, commonly nitrate, phosphate, carbonate or chloride. In these materials, divalent cations are partially replaced by trivalent cations, thus generating positive charges that are neutralized by anions and water molecules[2,3].

These materials are applied in catalysis, ion exchange, adsorption, photochemistry, electrochemistry, etc[4,5]. Recent works have reported the potential of these compounds in agriculture as matrices for storage and slow release of agrochemicals, such as nutrients, herbicides and plant growth regulators[6-13].

Cardoso *et al.*[6] intercalated 2,4-D; MCPA, and Picloram molecules in release tests performed in leaching columns and bioassays. When LDHs were compared with pure herbicides, leaching test results showed that the release is slow when the molecules are intercalated. For the bioassays, results showed that herbicide molecules intercalated in LDH presented the same pre-emergence control efficiency on *Lepidium sativum* as the pure herbicide molecules.

Hafez *et al.*[7] intercalated gibberellic acid (GA) in MgAl-LDH (GA-LDH). The study aimed to verify the slow release of GA in different solutions (pH = 3 and pH = 7) and the degradation of the substance in two soils (sandy and medium texture). The GA-LDH results were compared to pure GA. The authors showed that GA-LDH is more effective than pure GA, since pure GA crystallizes rapidly. After 24 hours of reaction, only 4.5% and 10.4% of GA was released in solutions of pH = 3 and pH = 7. After this period, the hormone becomes insoluble and no longer reacts in the medium. After 24 hours of reaction, the GA-LDH released 80% of GA into the solution at pH = 3 and 60% at pH = 7. In addition, it maintained a slow release until 6 days after the start of the reaction. Soil degradation tests showed that the intercalation increased the GA lifetime in the soil compared to pure GA. The pure GA remained for 6 days in the medium texture soil and 10 days in the sandy soil. After the intercalation, the period of GA in the soil increased to 20 days for the medium texture soil and 28 days for the sandy texture soil.

Silva *et al.*[14] and Silva *et al.*[15] synthesized LDHs intercalated with NO_3^- anions, varying the molar ratios of Mg^{2+}:Al^{3+} and Mg^{2+}:Fe^{3+}. In both works, the authors concluded LDHs presented protection for intercalated NO_3^- anions with potential uses as matrices for slow release of fertilizers.

Phosphorus (P) is an essential element for food production. P is a limited resource that has been inappropriately exploited, causing high pressure on worldwide reservese[16,17]. In recent years, problems related to P have been addressed in several

*e-mail: luizpaulo.figueredo@gmail.com

works, which have proposed strategies for dealing with the consequences of the uncontrolled use of this element in agriculture[18-23]. P scarcity is one of the biggest challenges of global sustainability in the 21st century, which directly affects food production and safety systems in the world[24]. Therefore, studies on improving the use of P have increased in recent years.

In many countries, mainly those in tropical regions, soils present low P availability because of the adsorption and fixation of this element by iron and aluminum oxides[25]. In these regions, high P content is usually applied for soil correction rather than plant nutrition[24-26].

The reduced contact between the phosphate ions and the soil mineral phase reduces the adsorption reactions/fixation of P by the soil[27,28]. Thus, an alternative for improving P performance in cultures is the development of sources to provide a physical protection for phosphate ions, in order to slow the release of these ions to plants. This physical protection can be created by the intercalation of phosphate ions in LDHs[29-33].

Because of the need to develop new technologies to increase the efficiency of phosphate fertilizers, the objectives of this work were as follows: (*i*) synthesis and characterization of MgAl-LDHs, MgFe-LDHs and MgAlFe-LDHs containing phosphate ions; and (*ii*) evaluation of P release kinetics in the prepared materials. These LDHs were prepared with different molar ratios of M^{2+} and M^{3+} cations. The produced materials were characterized by powder X-ray diffraction (PXRD), Fourier transform infrared spectroscopy with accessory of attenuated total reflectance (FTIR-ATR), Raman spectroscopy analyses and specific surface area by adsorption of N_2 (BET). The contents of C, N and H in the LDHs were determined by elementar analysis. For the prepared LDHs, P release kinetics were evaluated in an adaptation method stirred-flow.

2. Materials and Methods

2.1 Experimental Part

All reagents used in this work presented analytical degree of purity: $Mg(NO_3)_2 \cdot 6H_2O$, $Fe(NO_3)_3 \cdot 9H_2O$, $Al(NO_3)_3 \cdot 9H_2O$, KNO_3, K_2HPO_4, and NaOH. The water used in all reactions was distilled, deionized and decarbonated in a Milli-Q® Integral Water Purification System.

2.2 Synthesis of Layered Double Hydroxides

Initially, five pristine LDHs were synthesized with molar ratios ranging between M^{2+} and M^{3+} cations. All pristine LDHs were intercalated with NO_3^- anions. These materials were named Mg_2Al-LDH, Mg_3Al-LDH, Mg_2Fe-LDH, Mg_3Fe-LDH, and $Mg_2Fe_{0.5}Al_{0.5}$-LDH. The pristine LDHs were synthesized by the coprecipitation method at pH constant[4]. To prepare the material, 500 mL of a solution containing M^{2+} and M^{3+} cations in different molar ratios (Table 1) were slowly added drop by drop to 290 mL of a solution containing 1.48 mol L^{-1} of KNO_3. During this time, the suspension formed was kept under agitation in an N_2 atmosphere. A solution containing 2.00 mol L^{-1} of NaOH was added simultaneously to maintain a constant pH (± 0.5). The cations, molar ratio, number of mols and anions used in the synthesis of the pristine LDHs are shown (Table 1).

After the synthesis, the suspension was hydrothermally treated at 65°C during 24 h. After the hydrothermal treatment, the precipitate was filtered and washed with H_2O. The solid material obtained was freeze-dried for 120 h. After drying, the material was triturated and passed through an 80-mesh sieve to homogenize the particle sizes.

After synthesizing the pristine LDHs, the materials were subjected to an ion exchange reaction in solution for the incorporation of phosphate anions. The anion exchange in solution method was used for the incorporation of phosphate anions. In this method, 2.00 g of LDH precursor was suspended in 200 mL of a solution containing 1.00 mol L^{-1} of K_2HPO_4. The formed suspension was kept under agitation and atmosphere of N_2 for 24 h at 65 °C. At the end of the exchange reaction, the material was filtered again, washed and vacuum-dried in the presence of silica gel at room temperature. After the anion exchange reaction (Table 1), the names of pristine LDHs were changed to Mg_2Al-LDH-P, Mg_3Al-LDH-P, Mg_2Fe-LDH-P, Mg_3Fe-LDH-P, and $Mg_2Fe_{0.5}Al_{0.5}$-LDH-P.

Table 1. List of cations, anions, molar ratio of cations and number of mols used for pristine LDHs

LDHs	Cations	*Anions	Molar Ratio M^{2+}/M^{3+}	**Mols of M^{2+}	Mols of M^{3+}
Mg_2Al-LDH	$Mg^{2+}$and Al^{3+}	NO_3-	2:1	0.250	0.125
Mg_3Al-LDH	$Mg^{2+}$and Al^{3+}	NO_3-	3:1	0.375	0.125
Mg_2Fe-LDH	$Mg^{2+}$and Fe^{3+}	NO_3-	2:1	0.250	0.125
Mg_3Fe-LDH	$Mg^{2+}$and Fe^{3+}	NO_3-	3:1	0.375	0.125
$Mg_2Fe0.5Al0.5$-LDH	Mg^{2+}, $Fe^{3+}$and Al^{3+}	NO_3-	2:0.5:0.5	0.250	0.0625***

*Solution prepared from 0.428 mols of NO_3- in 290 mL of H_2O.

**Solution prepared in 250 mL of H_2O.

***0.0625 mols of each trivalent cation were added (Al^{3+} and Fe^{3+}).

2.3 Characterization of the LDHs

The quantities of C, N, and H in LDHs were determined by elemental analysis. Chemical analyses were done to quantify the total levels of LDH constituent elements. Metals were determined by inductively coupled plasma atomic emission spectroscopy (ICP-OES). P quantities contained in LDHs and in the solution after the kinetics experiments were determined by molecular absorption spectrometry in the UV-Vis region, as described by Braga and Defelipo[34].

In Brazil, phosphate fertilizers must contain minimum guarantees of P_2O_5 quantities as determined in H_2O, 2% citric acid and neutral ammonium citrate (NAC). To compare the various LDHs synthesized and the commercial sources of P, P_2O_5 in H_2O, 2% citric acid and NAC+H_2O were analyzed in accordance with the methodology described in AOAC[35].

The LDHs were characterized by powder X-ray diffraction (PXRD), Fourier transform infrared spectroscopy with accessory of attenuated total reflectance (FTIR-ATR), analyses of Raman spectroscopy and specific surface area through adsorption of gaseous N_2 (BET).

PXRD analyses were performed with a Shimadzu X-ray diffractometer, XRD 6000, with a copper cathode lamp (λ = 0.154 nm) and a graffiti monochromer to select the copper emission region, with potential source of 40 kV and current of 40 mA. The scanning rate of 0.01° every 10 s was used to determine the parameters of unitary cells of LDHs. The sweeping 2θ ranged from 4 to 70º.

FTIR-ATR analyses were conducted with a Jasco spectrophotometer, FTIR 4100. The spectra were obtained with 216 scans, in a wavenumber range from 4000 to 400 cm^{-1} and resolution of 4.0 cm^{-1}.

Raman measurements were performed in a Renishaw inVia confocal Raman microscope. The spectra were obtained through excitation with a near infrared laser line (λ = 785 nm) at 1.5 mW using a 50X standard objective lens. Fluorescence correction (background) was performed by removing the baseline using the baseline correction and smoothing filter functions in the software Origin 8.0.

The determination of the specific surface area (BET) was performed by the adsorption of N_2 gas in the sample using a Quantachrome analyzer, model Nova 2200e. The samples were degassed under vacuum at high temperature to remove H_2O and other volatile compounds. After degassing, the sample was transferred to the analysis module, where N_2 gas was injected into the interior of the cell to provide adsorption measures of N_2.

2.4 Kinetics of P Release

An adapted stirred-flow method, described by Strawn and Sparks[36], was used for the kinetics of P release experiments. The analyses system has a reaction chamber containing two filters. One of them has a 0.45 µm cellulose membrane and the other has Teflon with 25 mm pores. Both are used to retain the sample within the chamber. The chamber was placed on a magnetic stirrer (100 rpm) and coupled to a peristaltic pump, generating a flow of 1 mL min^{-1}. A fraction collector was coupled to the chamber outlet. Ultrapure H_2O was used as extractor. Approximately 2.00 mg of LDH was put into the agitation chamber and the pumped extraction solution was collected in the outlet of the system every 2 min up to 30 min, after that, every 6 min up to 110 min, and then each 10 min up to 150 min after the beginning of the flow. The P extracted from the samples, which was in the fractions, was determined as described by Braga and Defelipo[34]. For this determination, 0.5 mL of the sample collected in the stirred-flow was pipetted into 25 mL plastic cups and added to 4.5 mL of deionized H_2O. Immediately afterward, 5 mL of a working reagent composed of ammonium molibidate 0.01 mol L^{-1}, bismuth subcarbonate 0.01 mol L^{-1} and 1.6 g ascorbic acid were added. After 30 min, following the total blue color development, the samples were read on a UV-VIS spectrometer at a wavelength of 725 nm. The P contents P collected at different times in the stirred-flow assay were used to elaborate the mathematical model that best fitted the P release. The software CurveExpert version 1.4 was used to build the models.

3. Results and Discussion

3.1 Chemical Characterization

The values of molar ratio of M^{2+}/M^{3+} cations present in the layers were close to those added during the synthesis: Mg_2Al-LDH (Mg/Al = 2.2); Mg_3Al-LDH (Mg/Al = 3.3); Mg_2Fe-LDH (Mg/Fe = 1.9); Mg_3Fe-LDH (Mg/Fe = 2.8), and $Mg_2Fe_{0.5}Al_{0.5}$-LDH (Mg/FeAl) = 2.1). These values show that there was no lixiviation of cations during the synthesis process.

The amounts of C, H, N and P for pristine LDHs and LDHs-P are shown in Table 2. The LDHs of the Mg-Al system presented higher amounts of anions, both NO_3^- and phosphate. It was also possible to verify, for the MgAl-LDHs and MgFe-LDHs systems, that the molar ratio $M^{(2+)}/M^{(3+)}$ increased from 2:1 to 3:1, reducing the amount of intercalated NO_3^- and phosphate.

This reduction is related with the charge density of the materials; the lower the molar ratio, the higher the load density of the layer, which increases the number of intercalated anions between inorganic layers[37].

Results showed that the ionic exchange occurred in the solution and phosphate anions were able to replace part of intercalated NO_3^- anions. The P values obtained after the exchange reaction are close to those reported in the literature. Gillman *et al.*[38] used MgAl-LDH and different concentrations of phosphate in the exchange reactions and obtained materials with up to 62 mg g^{-1} of P. Triantafyllidis

Table 2. Contents of C, H, N and P of different LDHs

LDHs	Elements (mg/g)			
	C	H	N	P
		Pristine LDHs		
Mg_2Al-LDH	6.70	30.50	48.20	-
Mg_3Al-LDH	5.10	33.00	40.40	-
Mg_2Fe-LDH	8.20	28.80	20.20	-
Mg_3Fe-LDH	7.60	31.70	23.50	-
$Mg_2Fe_{0.5}Al_{0.5}$-LDH	5.60	26.40	42.26	-
		LDHs-P		
Mg_2Al-LDH-P	8.90	36.90	0.30	64.00
Mg_3Al-LDH-P	8.80	36.70	1.20	63.00
Mg_2Fe-LDH-P	10.60	29.50	2.50	43.20
Mg_3Fe-LDH-P	12.00	31.10	3.60	32.60
$Mg_2Fe_{0.5}Al_{0.5}$-LDH-P	11.00	31.50	1.00	41.80
		LDHs-P Formulas		
Mg_2Al-LDH-P	$Mg_{0.69}Al_{0.31}(OH)_2(HPO_4^{2-})_{0.309}(NO_3^-)_{0.001}\cdot 1.18H_2O$			
Mg_3Al-LDH-P	$Mg_{0.77}Al_{0.23}(OH)_2(HPO_4^{2-})_{0.226}(NO_3^-)_{0.004}\cdot 1.13H_2O$			
Mg_2Fe-LDH-P	$Mg_{0.65}Fe_{0.35}(OH)_2(HPO_4^{2-})_{0.330}(NO_3^-)_{0.020}\cdot 1.30H_2O$			
Mg_3Fe-LDH-P	$Mg_{0.74}Fe_{0.26}(OH)_2(HPO_4^{2-})_{0.234}(NO_3^-)_{0.026}\cdot 1.19H_2O$			
$Mg_2Fe_{0.5}Al_{0.5}$-LDH-P	$Mg_{0.68}Al_{0.15}Fe_{0.17}(OH)_2(HPO_4^{2-})_{0.311}(NO_3^-)_{0.007}\cdot 1.20H_2O$			

et al.[39] used MgAl, MgFe, and MgAlFe-LDHs and obtained materials with approximately 80 mg g^{-1} of P.

For Crepaldi and Valim[37], one of the main hindrances to ionic exchange reaction in solution is the precursor anion content that remains after the reaction. In agriculture however, the residual N content in the synthesized LDHs after exchange reaction by phosphate is a desirable characteristic. Nitrogen is an essential element for plants; thus, LDH-P can be a fertilizer and a source of N and P for plants.

The contents of total P_2O_5, in H_2O, 2% citric acid and NAC extractors are shown (Table 3). In relation to the P fraction extracted from different extractors (H_2O, 2% citric acid and NAC), MgAl-LDHs presented the lowest extracted amount for all three extractors. The use of H_2O as an extractor can determine only the most soluble forms of P. The 2% citric acid solution extracts low solubility forms, such as P-Ca, in addition to the soluble forms. The NAC solution is able to extract low solubility forms linked with Fe and Al[40].

As expected, all LDHs presented no solubility in H_2O and from average to high solubility in 2% citric acid and NAC. Such characteristics are very similar to reactive sources such as thermophosphate[41]. Phosphate sources of high H_2O solubility, such as triple superphosphate, simple superphosphate and mono ammonium phosphate, suffer huge losses of P due to adsorption abilities of tropical soils. Sources with reactive characteristics are a good alternative under these conditions because of the slow-release effect of these materials[42]. It is worth highlighting however that source efficiency is affected by not only reactivity, but also by soil and plant factors[43]. This suggests that LDHs can become a potential source of slow-release P in agriculture, once reactive sources show good agronomic efficiency[44,45].

3.2 Powder X-Ray Diffraction (PXRD)

The diffractograms of pristine LDHs are shown in Figure 1. These diffractograms show basal peaks (00*l*), (003) and (006), which indicate the presence of lamellar materials, such as hydrotalcite. Using Bragg's equation ($n\cdot\lambda = 2\cdot d\cdot \sin\theta$) and the average values of 2θ of the basal peaks (00*l*) of each LDH, it was possible to calculate the basal spacing *d* (spacing between two adjacent layers) of these materials. The obtained *d* values were 0.89; 0.88; 0.79; 0.79, and 0.81 nm for Mg_2Al-LDH, Mg_3Al-LDH, Mg_2Fe-LDH, Mg_3Fe-LDH, and $Mg_2Fe_{0.5}Al_{0.5}$-LDH, respectively. These values concur with those reported in the literature for intercalation of NO_3^- in LDHs[46,47]. All synthesized materials presented good structural organization and phase purity. LDH-5, with three different cations in the layers, presented poor crystallinity compared to the others.

For Mg_3Al-LDH and Mg_3Fe-LDH, the materials with the cation ratio of M^{2+}:M^{3+} = 3:1 showed more intense basal peaks (00*l*), indicating higher crystallinity. The lower proportion of trivalent cation in the layers increased the crystallinity of the materials. The lower the number of cations M^{2+} replaced by M^{3+}, the lower the distortion of the layers and consequently the better the arrangement of stacking for the structure[15,48].

Table 3. Contents of total P_2O_5, in water, 2% citric acid and neutral ammonium citrate (NAC)

Material	P_2O_5 Total	*Soluble P_2O_5 in H_2O	*P_2O_5 in 2% citric acid	*P_2O_5 in NAC
		(%)		
Mg_2Al-LDH-P	7.32	12.80	85.31	17.50
Mg_3Al-LDH-P	7.21	16.04	72.06	18.41
Mg_2Fe-LDH-P	4.94	33.70	96.29	35.18
Mg_3Fe-LDH-P	3.73	46.50	78.52	48.46
$Mg_2Fe_{0.5}Al_{0.5}$-LDH-P	4.78	26.00	85.26	32.05

*In relation to Total P.

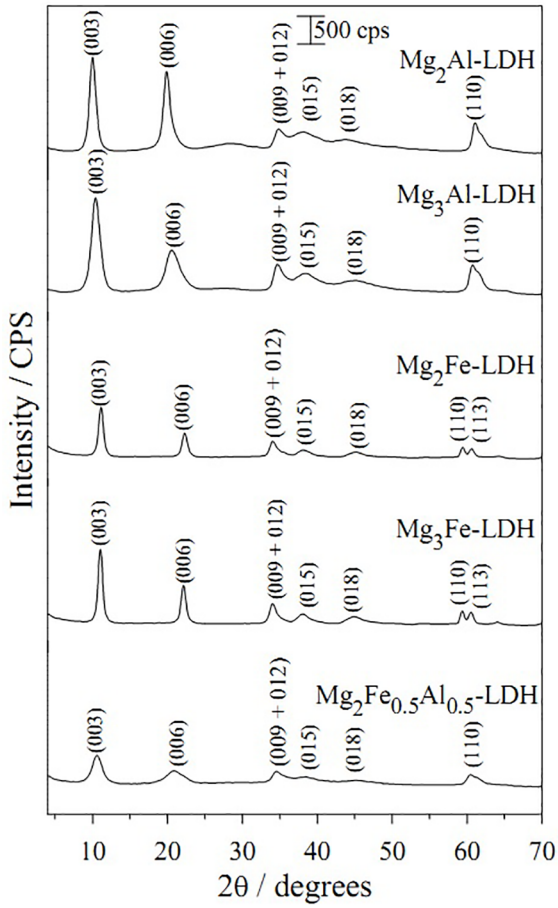

Figure 1. Diffractograms of pristine LDHs: Mg_2Al-LDH, Mg_3Al-LDH, Mg_2Fe-LDH, Mg_3Fe-LDH, $Mg_2Fe_{0.5}Al_{0.5}$-LDH

The synthesized $Mg_2Fe_{0.5}Al_{0.5}$-LDH showed lower crystallinity when compared with the LDHs synthesized with two different cations. This result is highlighted by the lower intensity of the basal peaks in the diffractogram of $Mg_2Fe_{0.5}Al_{0.5}$-LDH. The presence of three different types of cations in the layers results in lower structural organization when compared with LDHs synthesized with two different types of cations.

Figure 2 presents the diffractograms of pristine LDHs subjected to anionic exchange reaction in solution. Mg_2Al-LDH-P and Mg_3Al-LDH-P presented significant changes in the diffraction patterns, compared to pristine Mg_2Al-LDH and

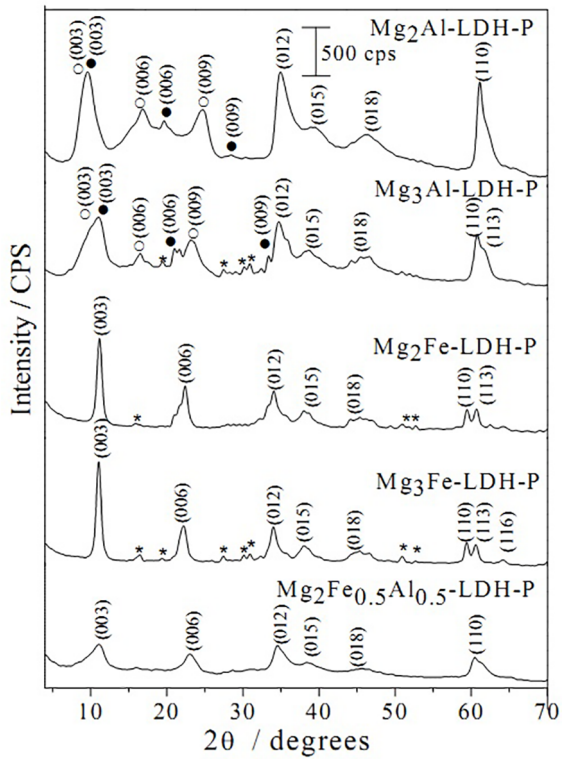

Figure 2. Diffractograms of LDHs after exchange reactions: Mg_2Al-LDH-P, Mg_3Al-LDH-P, Mg_2Fe-LDH-P, Mg_3Fe-LDH-P, $Mg_2Fe_{0.5}Al_{0.5}$-LDH-P. (○) Phase one; (●) Phase two; ★ K_2HPO_4

Mg_3Al-LDH. Two phases are found for these materials. In the first phase, the basal peaks are described in the diffractogram as ○(003) and ○(006) and the basal spacing values found for this phase were 0.62 nm for Mg_2Al-LDH-P and 0.64 nm for Mg_3Al-LDH-P. In the second phase, the basal peaks are marked in the diffractogram as ●(003), ●(006), and ●(009). The basal spacing values found for this phase were 0.92 nm for Mg_2Al-LDH-P and 0.81 nm for Mg_3Al-LDH-P. The obtained results for C, N, and P quantifications are presented in Table 2. After the ionic exchange reaction, the LDHs presented significant amounts of N and C. As expected, the presence of N suggests the exchange reaction between nitrate by phosphate anions was incomplete. The presence of CO_3^{2-} is due to the contamination by atmospheric CO_2. Even when all reactions (coprecipitation and exchange) are conducted in an inert environment (N_2), handling during washing, drying and

analyses exposes LDHs to the air. Due to the high basicity presented by these materials, contact with atmospheric CO_2 causes them to be absorbed and incorporated to LDH in the CO_3^{2-} form[49]. Thus, there may be co-intercalation of NO_3^-, phosphate, and CO_3^{2-} anions in LDHs subjected to anionic exchange reactions.

In the literature, the basal spacing values found for LDHs intercalated with NO_3^- are 0.87 nm[49,50] and 0.89 nm[51]. For LDHs intercalated with CO_3^{2-}, the values are 0.76 nm[49,52] and 0.75 nm[53]. LDHs intercalated with phosphate have very different basal space values: 0.84 nm[54], and 0.78 nm, 0.80 nm, 1.19 nm[55] and 1.11 nm[12]. These different basal space values for the intercalation of phosphate are attributed to the different positions adopted by these anions between the inorganic layers (perpendicular, inclined and planar). Factors such as the charge density of the layers, hydration state and synthesis methods used can affect the position of the anions between the layers.

For Mg_2Fe-LDH-P and Mg_3Fe-LDH-P, the calculated basal spacing values were 0.79 nm and 0.78 nm. For these LDHs, the amount of P found in relation to nitrogen (Table 2) is significant, which suggests phosphate ions can also be intercalated. For the MgAl-HPO_4 system, Frost *et al.*[56] found basal spacing values between 0.78 nm and 1.19 nm. For the Mg-Fe system, Triantafyllidis *et al.*[39] found basal spacing values around 0.77 nm.

3.3 Fourier transform infrared spectroscopy with accessory of attenuated total reflectance (FTIR-ATR)

FTIR-ATR spectra for pristine LDHs are presented in Figure 3. All spectra have a wide band in the 3400 cm^{-1} region. The presence of these bands is attributed to -OH stretching of H_2O molecules and to hydroxyl groups present in the layers. The spectrum also presents a strong band in the 1763 cm^{-1} region, referring to C=O bonds, which allows inferring on the presence of CO_3^{2-} in LDHs.

The spectra for the pristine LDHs also show the presence of bands in the 1350 cm^{-1} region, attributed to vibration modes (ν3) of NO_3^-. In LDH, it is possible to find two types of nitrate, with bands in the 836 cm^{-1}, 1380 cm^{-1} and 1763 cm^{-1} regions that present "free" NO_3^- and in the 825 cm^{-1}, 840 cm^{-1} 1050 cm^{-1} and 1425 cm^{-1} regions that represent "non-free" NO_3^-[48,57]. Figure 4 shows the spectra for LDHs after the exchange reaction. These spectra also present wide bands in the 3400 cm^{-1} region, characteristic of the presence of -OH groups. The presence of phosphate can be evidenced by the bands in the 1050 cm^{-1}, 870 cm^{-1} and 550 cm^{-1} regions, which correspond to ν3(PO_4^{3-}); ν1(PO_4^{3-}) and ν4(PO_4^{3-}) vibrations[58]. The band in the 1350 cm^{-1} region can be attributed to the vibration modes of NO_3^- or CO_3^{2-}. In the literature, several works have reported the overlap of CO_3^{2-} and NO_3^- bands in the region ranging from 1350 to 1400 $cm^{(-1)}$ in LDHs[59-63].

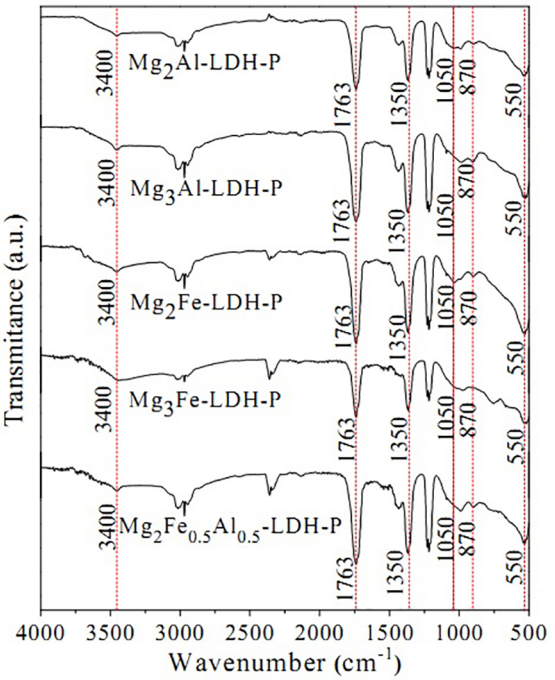

Figure 3. FTIR-ATR spectra of the pristine LDHs: Mg_2Al-LDH, Mg_3Al-LDH, Mg_2Fe-LDH, Mg_3Fe-LDH, $Mg_2Fe_{0.5}Al_{0.5}$-LDH

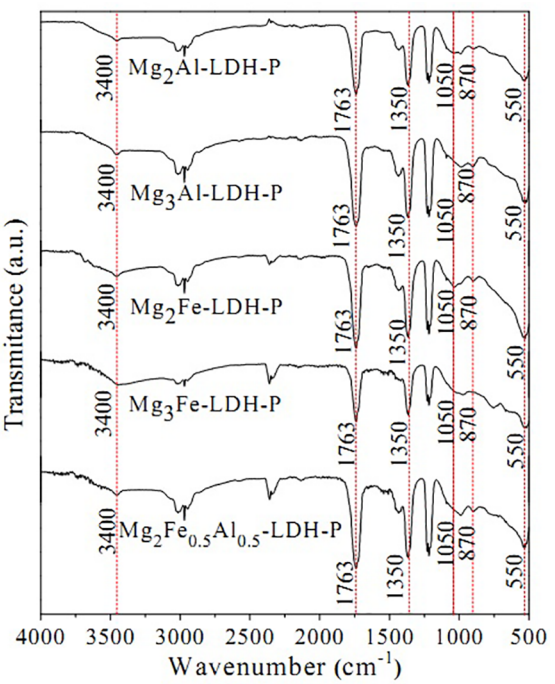

Figure 4. FTIR-ATR spectra of LDHs after anionic exchange reaction: Mg_2Al-LDH-P, Mg_3Al-LDH-P, Mg_2Fe-LDH-P, Mg_3Fe-LDH-P, $Mg_2Fe_{0.5}Al_{0.5}$-LDH-P

3.4 Raman Spectroscopy

Figure 5 presents the Raman spectra for pristine LDHs. The spectra show bands in the 470 cm^{-1} region, which are attributed to the vibration of connections Al-O-Al and Fe-

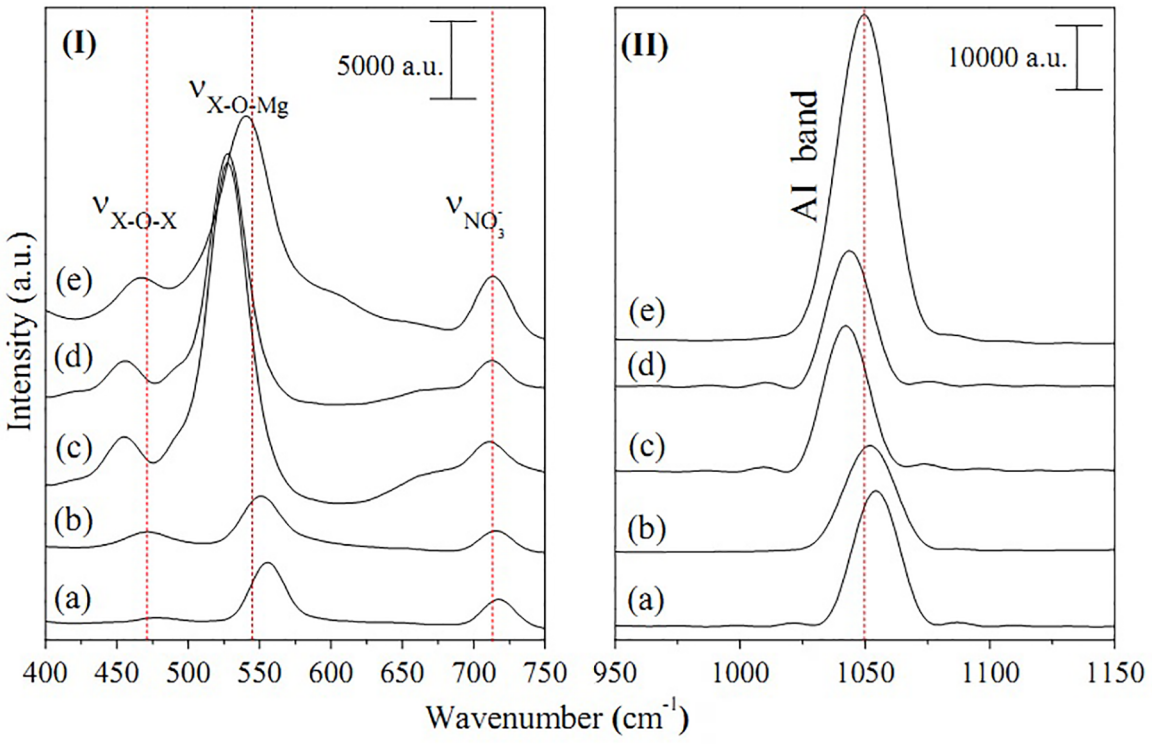

Figure 5. Raman spectra of pristine LDHs : (I) 400 - 750 cm^{-1} region and (II) 950 - 1150 cm^{-1} region for (a) Mg_2Al-LDH, (b) Mg_3Al-LDH, (c) Mg_2Fe-LDH, (d) Mg_3Fe-LDH, (e) $Mg_2Fe_{0.5}Al_{0.5}$-LDH. In the band index, X refers to Fe or Al, depending on the sample. The AI bands are associated to the anion intercalated vibrations

O-Fe present in the layers of the MgAl-LDH, MgFe-LDH and MgFeAl-LDH systems.

In the 550 cm^{-1} region, the bands refer to the signature octahedral structure of brucite-type layers, i.e. Al-O-Mg or Fe-O-Mg. The 710 cm^{-1} band is specifically attributed to NO_3^- ion, while in the 1050 cm^{-1} region, it corresponds to the anion intercalated (independent of the type of anion) in LDH like materials[64-69].

Figure 6 shows the Raman spectra for LDHs subjected to anionic exchange reaction. In these spectra, it is possible to see the permanence of bands in the 470 cm^{-1} and 550 cm^{-1} regions, corresponding to the lamellar structure of LDHs. Except for LDH-5P, the band is not present in the 710 cm^{-1} region, referring to NO_3^-. The presence of phosphate is evidenced by the emergence of bands in the region between 940 cm^{-1} and 960 cm^{-1}[67]. Slight changes can also be observed in the positions of the bands of the materials subjected to the exchange reaction in relation to pristine LDHs, such as in bands located in the 1050 cm^{-1} region. These results are in line with those presented by Palmer *et al.*[70], which show the form and position of Raman bands depending on the nature and concentration of the intercalated anions in LDHs.

3.5 Specific Surface Area (BET method)

Table 4 presents the measurements of specific surface area, pore volume and mean pore diameter for pristine LDHs and LDHs-P. The increased molar ratio between M^{2+}/M^{3+} cations present in the layers reduced the specific surface area, pore volume and mean pore diameter. For MgAl-LDHs, the reduction was 1.44 times the specific surface area and 1.50 times the pore volume. For MgFe-LDHs, both specific surface area and pore volume were reduced by 1.23.

The specific surface area values found in the literature for LDHs generally range from 50 to 80 $m^2\ g^{-1}$. Some works however found values of 200 $m^2\ g^{-1}$[71,72]. The reduction of porosity and specific surface area with increased molar ratio M^{2+}/M^{3+} in LDHs was previously reported by Jaynes and Vance[73], Di Cosimo *et al.*[74], You *et al.*[75], and Cantrell *et al.*[52]. The increased molar ratio reduces the charge density of the layers, and consequently, the specific surface area of these materials. For all LDHs, the sorption and desorption N_2 isotherms (presented in supplementary material) are type II, according to IUPAC (International Union of Pure Applied Chemistry), with close hysteresis, typical of mesoporous materials (pore size between 2-50 nm)[76].

3.6 Kinetics of P Release

LDHs were subjected to release tests of P in H_2O. The pH values of the suspensions before the stirred-flow experiments were Mg_2Al-LDH-P = 7.85; Mg_3Al-LDH-P = 8.15; Mg_2Fe-LDH-P = 8.37; Mg_3Fe-LDH-P = 9.01, and $Mg_2Fe_{0.5}Al_{0.5}$-LDH = 8.81. The cumulative rate releases and

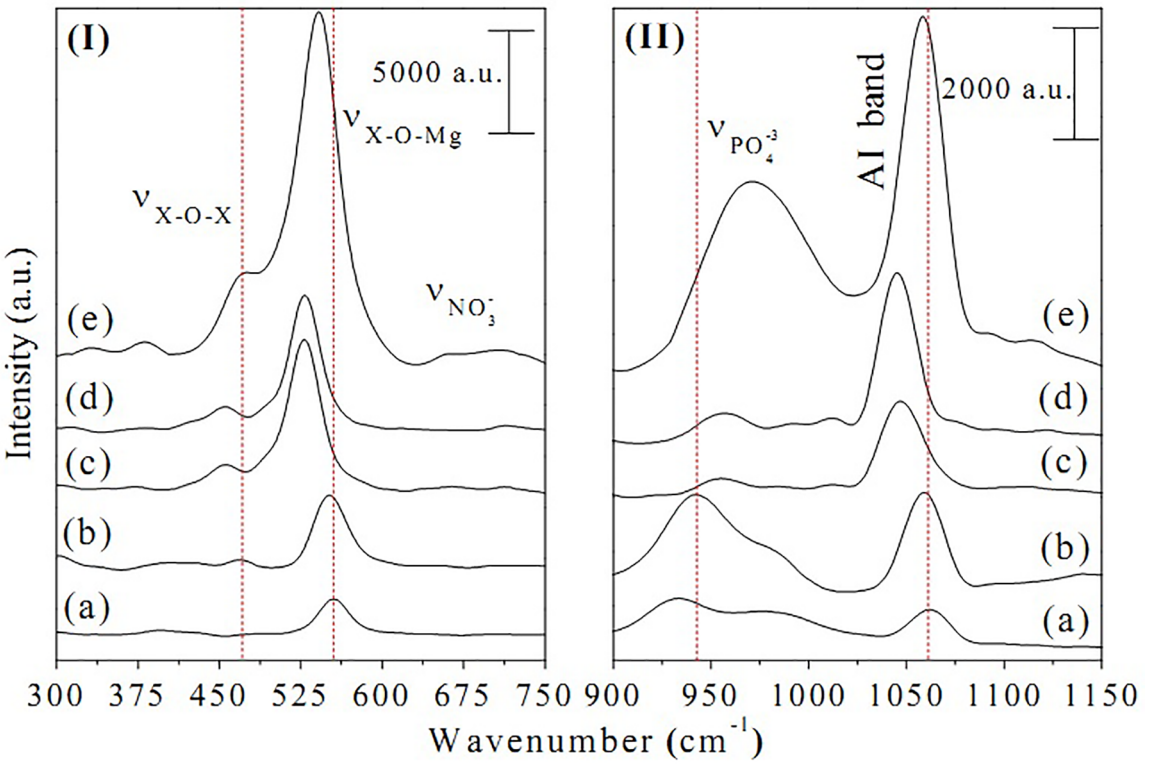

Figure 6. Raman spectra of LDHs after exchange reaction: (I) 400 - 750 cm^{-1} region and (II) 900 - 1150 cm^{-1} region for (a) Mg_2Al-LDH-P, (b) Mg_3Al-LDH-P, (c) Mg_2Fe-LDH-P, (d) Mg_3Fe-LDH-P, (e) $Mg_2Fe_{0.5}Al_{0.5}$-LDH-P. In the band index, X refers to Fe or Al, depending on the sample. The AI bands are associated to the anion intercalated vibrations.

Table 4. Specific surface area and pore volume of different LDHs

Pristine LDHs	S.S.A.* (m^2/g)	P.V.** cm^3/g	LDHs-P	S.S.A.* m^2/g	P.V.** cm^3/g
Mg_2Al-LDH	76.0	2.64	Mg_2Al-LDH-P	19.7	7.69
Mg_3Al-LDH	52.6	1.76	Mg_3Al-LDH-P	10.0	3.57
Mg_2Fe-LDH	189.0	76.5	Mg_2Fe-LDH-P	61.2	24.4
Mg_3Fe-LDH	153.0	62.0	Mg_3Fe-LDH-P	58.4	23.2
$Mg_2Fe_{0.5}Al_{0.5}$-LDH	47.9	1.93	$Mg_2Fe_{0.5}Al_{0.5}$-LDH-P	12.5	4.89

**S.S.A = Specific Surface Area;*

***P.V.* = Pore Volume

P release profiles in solution for Mg_2Al-LDH-P and Mg_3Al-LDH-P over time are presented in Figure 7. For all LDHs studied, the curves that represent the profile of P release in solution are represented by two distinct and complementary moments: (*i*) fast release and (*ii*) slow release. The initial fast release is linked with phosphate adsorbed in the surface of LDHs crystallites, which are promptly exchanged. Then, the release slows because of the exchange reaction of the intercalated phosphate with the anions present on reaction medium.

The P profiles release and cumulative release rates for Mg_2Al-LDH-P and Mg_3Al-LDH-P are shown in Figure 7. Mg_2Al-LDH-P showed better adjustment to the Hoerl model, as did Mg_3Al-LDH-P to Vapor Pressure model. The adjustments were done using the equations obtained for each model. The turning point was also estimated, where the release rate of P becomes descendant and slower. In Mg_2Al-LDH-P, this change occurs at 22 min, while for Mg_3Al-LDH-P, this point is reached more rapidly, at 12 min. The cumulative rate of the two LDHs shows that Mg_2Al-LDH-P releases P more slowly than Mg_3Al-LDH-P. After 150 min of flow, Mg_2Al-LDH-P released approximately 60% of its total P content, while Mg_3Al-LDH-P released around 83% for the same amount of time.

Figure 8 shows the release profiles of P and cumulative release rates for Mg_2Fe-LDH-P and Mg_3Fe-LDH-P. The release profiles of P for Mg_2Fe-LDH-P and Mg_3Fe-LDH-P were adjusted for the Vapor Pressure and Hoerl modified

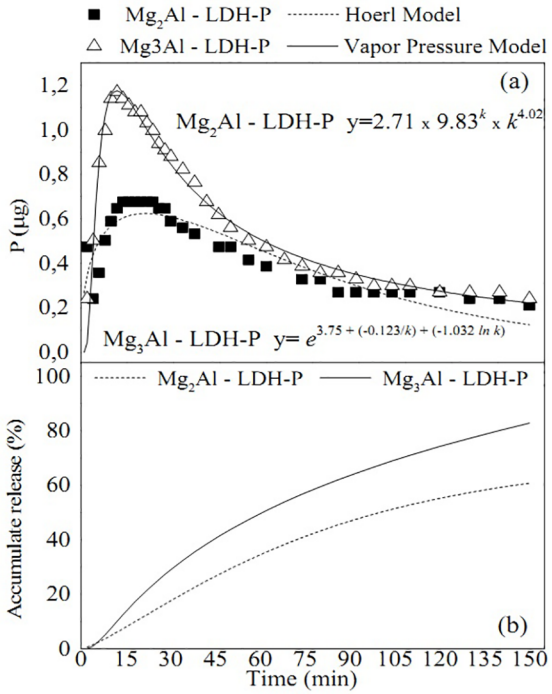

Figure 7. P release in solution of Mg_2Al-LDH-P and Mg_3Al-LDH-P in relation to the time. (a) release profile, (b) cumulative rate release.

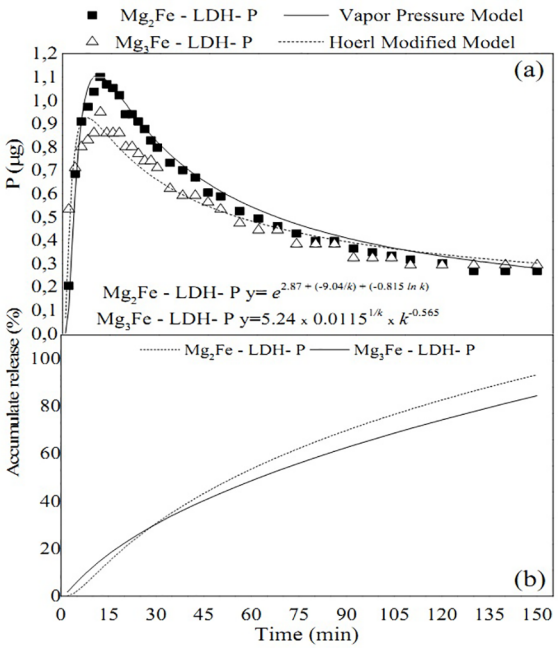

Figure 8. P release in Mg_2Fe-LDH-P and Mg_3Fe-LDH-P solutions in relation to time. (a) release profile, (b) cumulative release rate.

models. The turning point was reached at 11 min for Mg_2Fe-LDH-P and 8 min for Mg_3Fe-LDH-P. Despite reaching the change point more rapidly, Mg_3Fe-LDH-P presents lower declivity than Mg_2Fe-LDH-P, with a longer decline phase and consequently a slower release. The cumulative release rate of Mg_2Fe-LDH-Pand Mg_3Fe-LDH-P corroborates that Mg_3Fe-LDH-P has a slower release. At the end of 150 min of flow, Mg_2Fe-LDH-P had released around 93% of its total content of P, while Mg_3Fe-LDH-P released approximately 84%.

Figure 9 presents the release profile of P and the cumulative release rate for $Mg_2Fe_{0.5}Al_{0.5}$-LDH-P. $Mg_2Fe_{0.5}Al_{0.5}$-LDH-P had the same release profile with two distinct and complementary moments, as well as the previous ones. The Vapor Pressure model best represents the release profile of this LDH. It took $Mg_2Fe_{0.5}Al_{0.5}$-LDH-P 16 min to reach the maximum point of release. Compared to the other materials however, $Mg_2Fe_{0.5}Al_{0.5}$-LDH-P has a faster P release after entering the phase of descending release. The cumulative release rate shows that only $Mg_2Fe_{0.5}Al_{0.5}$-LDH-Pcompletely released its full amount of P. The cumulative release reached approximately 100% after 130 min of flow.

The Hoerl and Vapor Pressure models are variations of the exponential model. These models are extremely flexible and can be used in cases where other non-linear models fail. Due to the complexity of the medium and the number of variables involved, the Hoerl model has been used in studies to evaluate plants nutrition experiments with sufficient accuracy[77].

Comparatively, among the five LDHs-P studied, the Mg_2Al-LDH-P obtained better results from its release profile and cumulative release rate. The highest amount of P release in all LDHs-P occurred by exchange reactions. Once LDHs-P are in contact with water, they dissociate part of the hydroxyls from the layers[15] thus increasing the pH value of the suspensions. The pH values of the suspensions after the stirred-flow experiments were Mg_2Al-LDH-P =

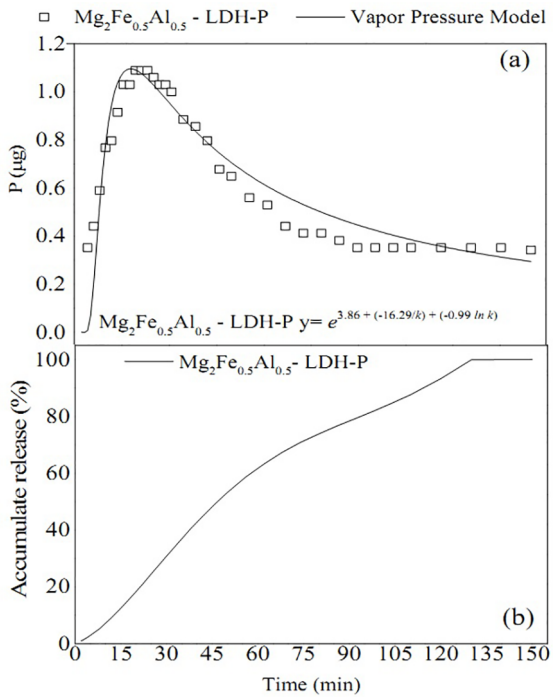

Figure 9. P release in $Mg_2Fe_{0.5}Al_{0.5}$-LDH solution in relation to time. (a) release profile. (b) cumulative release rate.

8.62; Mg_3Al-LDH-P = 9.15; Mg_2Fe-LDH-P = 9.92; Mg_3Fe-LDH-P = 9.88, and $Mg_2Fe_{0.5}Al_{0.5}$-LDH-P = 9.03. Under these pH values, atmospheric CO_2 dissolved in the LDH suspension and reacted with H_2O, producing CO_3^{2-}[37]. The CO_3^{2-} formed in suspension provides the exchange with phosphate intercalated in LDHs.

For Silva *et al*.[15], the differences in release rates are controlled by factors such as layer components, charge density of the layers, and size of crystallites. The different compositions and M^{2+}/M^{3+} molar ratios presented in this work also evidenced these characteristics. $Mg_2Fe_{0.5}Al_{0.5}$-LDH-P with three different cations in the layers promoted the formation of a material with higher structural disorder and lower crystallinity, as evidenced by PXRD measurements. The low crystallinity presented by this material provided a fast release rate compared to the other LDHs-P with better structural organization.

MgAl-LDHs-P released less P than the compounds with Fe^{3+}, which demonstrates that Al^{3+} retained phosphate in its structure with a stronger connection and thus lower possibility of displacing this anion. For the MgFe-LDHs-P, the amount of P initially released (fast moment) was higher than the amounts released in the samples containing Al^{3+}. This relationship suggests LDHs synthesized with Al^{3+} ions have better P retention capacity and that the release occurs gradually.

As suggested by Silva *et al*.[15], in addition to the physical protection of anions provided by intercalation, LDHs also contain a chemical protection called the "interlayer ionic barrier". Both are responsible for the gradual release of intercalated anions. These authors conducted a slow release study of NO_3^- intercalated in MgAl-LDHs and MgFe-LDHs. A solution of $NaHCO_3$ was used for the release test. According to the authors, the exchange of NO_3^- intercalated in LDHs by the CO_3^{2-} of the solution starts in the edges of the layers, where the newly exchanged CO_3^{2-} anions form a barrier that hinders the exit of NO_3^- located in the internal region of the layers and prevents its fast release.

The results obtained in this work demonstrate that LDHs are materials that can resolve problems related with P losses in tropical soils, due to the protection and gradual release of the phosphate ions they contain. With regard to P recycling, LDHs are also potential materials because they can incorporate phosphate anions from aqueous solutions and then be used in the soil as sources of P. There are several reports in the literature about the use of LDH for P removal from sewage sludge, in residual water and even in ocean water[32,78-81].

4. Conclusions

The results presented in this work showed that by using the co-precipitation method followed by the ionic exchange method in solution it was possible to synthesize LDH containing phosphate ions in different systems, with different types of cations and different molar ratios (M^{2+}:M^{3+}) between them (Mg_2Al, Mg_3Al, Mg_2Fe, Mg_3Fe and MgFeAl). In addition to significant amounts of P, the ionic exchange reaction produced materials with amounts of N and C. Among the LDHs obtained, Mg_2Al-LDH-P presented the highest amount of P. The contents of P_2O_5, extracted with H_2O, 2% citric acid and CNA + H_2O extractors, showed that LDHs-P have similar characteristics to reactive sources of P, such as commercial thermophosphates. In studies on the kinetics of P release, LDHs-P showed a gradual P release profile and Mg_2Al-LDH-P presented a slower release than the other materials. Likewise, LDHs presented structural and chemical characteristics that make them potential materials for use as storage matrices for slow P release. New studies and tests with plants and soils (bioassays) are being developed by our research group to try to validate this new LDH technology for use as a source of P. The development of a unique material able to solve all worldwide problems related to P in agriculture is not an easy task and may even be unfeasible. LDHs have characteristics however that make them potential materials for solving one or more aspects of this problem.

5. Acknowledgments

This study was supported by the Fundação de Amparo à Pesquisa do Estado de Minas Gerais - FAPEMIG, Conselho Nacional de Desenvolvimento Científico e Tecnológico - CNPq, and Rede Mineira de Química (RQ-MG).

6. References

1. Bellezza F, Nocchetti M, Posati T, Giovagnoli S, Cipiciani A. Synthesis of colloidal dispersions of NiAl, ZnAl, NiCr, ZnCr, NiFe, and MgFe hydrotalcite-like nanoparticles. *Journal of Colloid and Interface Science*. 2012;376(1):20-27.

2. De Roy A, Forano C, El Malki K, Besse JP. Anionic Clays: Trends in Pillaring Chemistry. In: Occelli ML, Robson HE, eds. *Synthesis of Microporous Materials*. Boston: Springer; 1992. p. 108-169.

3. Labajos FM, Rives V. Thermal Evolution of Chromium(III) Ions in Hydrotalcite-like Compounds. *Inorganic Chemistry*. 1996;35(18):5313-5318.

4. Cavani F, Trifirò F, Vaccari A. Hydrotalcite-type anionic clays: Preparation, properties and applications. *Catalysis Today*. 1991;11(2):173-301.

5. Li F, Duan X. Applications of Layered Double Hydroxides. In: Duan X, Evans DG, eds. *Layered Double Hydroxides*. Berlin Heidelberg: Springer; 2006. p. 193-223.

6. Cardoso LP, Celis R, Cornejo J, Valim JB. Layered double hydroxides as supports for the slow release of acid herbicides. *Journal of Agricultural and Food Chemistry*. 2006;54(16):5968-5975.

7. Hafez IH, Berber MR, Minagawa K, Mori T, Tanaka M. Design of a multifunctional nanohybrid system of the phytohormone gibberellic acid using an inorganic layered double-hydroxide material. *Journal of Agricultural and Food Chemistry*. 2010;58(18):10118-10123.

8. Hashim N, Hussein MZ, Isa I, Kamari A, Mohamed A, Jaafar AM, et al. Synthesis and controlled release of cloprop herbicides from cloprop-layered double hydroxide and cloprop-zinc-layered hydroxide nanocomposites. *Open Journal Inorganic Chemistry*. 2014;4(1):1-9.

9. Pavlovic I, González MA, Rodríguez-Rivas F, Ulibarri MA, Barriga C. Caprylate intercalated layered double hydroxide as adsorbent of the linuron, 2,4-DB and metamitron pesticides from aqueous solution. *Applied Clay Science*. 2013;80-81:76-84.

10. Li S, Shen Y, Xiao M, Liu D, Fan L. Synthesis and controlled release properties of ß-naphthoxyacetic acid intercalated Mg-Al layered double hydroxides nanohybrids. *Arabian Journal of Chemistry*. 2015. E-pub ahead of print.

11. Benício LPF, Silva RA, Lopes JA, Eulálio D, dos Santos RMM, De Aquino LA, et al. Layered Double Hydroxides: Nanomaterials for Applications in Agriculture. *Revista Brasileira de Ciência do Solo*. 2015;39(1):1-13.

12. Benício LPF, Constantino VRL, Pinto FG, Vergütz L, Tronto J, da Costa LM. Layered Double Hydroxides: New Technology in Phosphate Fertilizers Based on Nanostructured Materials. *ACS Sustainable Chemistry & Engineering*. 2017;5(1):399-409.

13. Bernardo MP, Moreira FKV, Ribeiro C. Synthesis and characterization of eco-friendly Ca-Al-LDH loaded with phosphate for agricultural applications. *Applied Clay Science*. 2017;137:143-150.

14. Da Silva V, Kamogawa MY, Marangoni R, Mangrich AS, Wypych F. Hidróxidos Duplos Lamelares para matrizes para fertilizantes de liberação lenta de nitrato. *Revista Brasileira de Ciência do Solo*. 2014;38(3):272-277.

15. Da Silva V, Mangrich AS, Wypych F. Liberação de nitrato de hidróxidos duplos lamelares como potenciais fertilizantes de liberação lenta. *Revista Brasileira de Ciência do Solo*. 2014;38(3):821-830.

16. Elser J, Bennett E. Phosphorus cycle: A broken biogeochemical cycle. *Nature*. 2011;478(7367):29-31.

17. Chowdhury RB, Moore GA, Weatherley AJ, Arora M. A review of recent substance flow analyses of phosphorus to identify priority management areas at different geographical scales. *Resources, Conservation and Recycling*. 2014;83:213-228.

18. Balemi T, Negisho K. Management of soil phosphorus and plant adaptation mechanisms to phosphorus stress for sustainable crop production: a review. *Journal of Soil Science and Plant Nutrition*. 2012;12(3):547-562.

19. Schoumans OF, Chardon WJ, Bechmann ME, Gascuel-Odoux C, Hofman G, Kronvang B, et al. Mitigation options to reduce phosphorus losses from the agricultural sector and improve surface water quality: A review. *Science of the Total Environment*. 2014;468-469:1255-1266.

20. Withers PJA, Elser JJ, Hilton J, Ohtake H, Schipper WJ, van Dijk KC. Greening the global phosphorus cycle: how green chemistry can help achieve planetary P sustainability. *Green Chemistry*. 2015;17(4):2087-2099.

21. Shepherd JG, Kleemann R, Bahri-Esfahani J, Hudek L, Suriyagoda L, Vandamme E, et al. The future of phosphorus in our hands. *Nutrient Cycling in Agroecosystems*. 2016;104(3):281-287.

22. Rosemarin A, Ekane N. The governance gap surrounding phosphorus. *Nutrient Cycling in Agroecosystems*. 2016;104(3):265-279.

23. Dodd RJ, Sharpley AN. Conservation practice effectiveness and adoption: unintended consequences and implications for sustainable phosphorus management. *Nutrient Cycling in Agroecosystems*. 2016;104(3):373-392.

24. Cordell D, Neset TSS. Phosphorus vulnerability: A qualitative framework for assessing the vulnerability of national and regional food systems to the multi-dimensional stressors of phosphorus scarcity. *Global Environmental Change*. 2014;24(1):108-122.

25. Eberhardt DN, Vendrame PRS, Becquer T, Guimarães MF. Influência da granulometria e da mineralogia sobre a retenção do fósforo em latossolos sob pastagens no Cerrado. *Revista Brasileira Ciência do Solo*. 2008;32(3):1009-1016.

26. Peñuelas J, Poulter B, Sardans J, Ciais P, van der Velde M, Bopp L, et al. Human-induced nitrogen-phosphorus imbalances alter natural and managed ecosystems across the globe. *Nature Communications*. 2013;4:2934.

27. Muukkonen P, Hartikainen H, Lahti K, Särkelä A, Puustinen M, Alakukku L. Influence of no-tillage on the distribution and lability of phosphorus in Finnish clay soils. *Agriculture, Ecosystems & Environment*. 2007;120(2-4):299-306.

28. Olibone D, Rosolem CA. Phosphate fertilization and phosphorus forms in an Oxisol under no-till. *Scientia Agricola*. 2010;67(4):465-471.

29. Ookubo A, Ooi K, Hayashi H. Preparation and phosphate ion-exchange properties of a hydrotalcite-like compound. *Langmuir*. 1993;9(5):1418-1422.

30. Costantino U, Casciola M, Massinelli L, Nocchetti M, Vivani R. Intercalation and grafting of hydrogen phosphates and phosphonates into synthetic hydrotalcites and a.c.-conductivity of the compounds thereby obtained. *Solid State Ionics*. 1997;97(1-4):203-212.

31. Khaldi M, Badreddine M, Legrouri A, Chaouch M, Barroug A, De Roy A, et al. Preparation of a well-ordered layered nanocomposite from zinc-aluminum-chloride layered double hydroxide and hydrogenophosphate by ion exchange. *Materials Research Bulletin*. 1998;33(12):1835-1843.

32. Chitrakar R, Tezuka S, Sonoda A, Sakane K, Ooi K, Hirotsu T. Adsorption of phosphate from seawater on calcined MgMn-layered double hydroxides. *Journal of Colloid and Interface Science*. 2005;290(1):45-51.

33. Ye L, Qu B. Flammability characteristics and flame retardant mechanism of phosphate-intercalated hydrotalcite in halogen-free flame retardant EVA blends. *Polymer Degradation and Stability*. 2008;93(5):918-924.

34. Braga JM, Defellipo BV. Determinação espectofotométrica de fósforo em extratos de solos e planta. *Revista Ceres*. 1974;21(113):7-85.

35. AOAC - Association of Analytical Chemists. *Official Methods of Analysis*. 15th ed. Arlington: AOAC; 1990.

36. Strawn DG, Sparks DL. Effects of Soil Organic Matter on the Kinetics and Mechanisms of Pb(II) Sorption and Desorption in Soil. *Soil Science Society America Journal*. 2000;64:144-156.

37. Crepaldi EL, Valim JB. Hidróxidos duplos lamelares: síntese, estrutura, propriedades e aplicações. *Química Nova*. 1998;21(3):300-311.

38. Gillman GP, Noble MA, Raven MD. Anion substitution of nitrate-saturated layered double hydroxide of Mg and Al. *Applied Clay Science*. 2008;38(3-4):179-186.

39. Triantafyllidis KS, Peleka EN, Komvokis VG, Mavros PP. Iron-modified hydrotalcite-like materials as highly efficient phosphate sorbents. *Journal of Colloid and Interface Science*. 2010;342(2):427-436.

40. Alcarde JC, Ponchio CO. A ação solubilizante das soluções de citrato de amônio e de ácido cítrico sobre fertilizantes fosfatados. *Revista Brasileira de Ciência do Solo*. 1979;3:173-178.

41. Sousa DMG, Lobato E, Rein TA. Adubação com Fósforo. In: Sousa DMG, Lobato E, eds. Cerrado: *Correção do Solo e Adubação*. Planaltina: EMBRAPA Cerrados; 2004. p. 147-168.

42. Quispe JFS. *Eficiência agronômica de fosfatos com solubilidade variável em água em solos distintos quanto a capacidade de fixação de fósforo*. [Dissertation]. Piracicaba: University of São Paulo (Esalq); 2004.

43. Khasawneh FE, Doll EC. The Use of Phosphate Rock for Direct Application to Soils. *Advances in Agronomy*. 1979;30:159-206.

44. Lacerda JJJ, Furtini Neto AE, Resende AV, Santos JZL, Carneiro LF, Oliveira CHC. Crop growth response and dynamics of inorganic phosphorus fractions after application of reactive Arad phosphate rock in Oxisol with different land use histories. *African Journal of Agricultural Research*. 2013;8(26):3454-3461.

45. Duarte RF, Santana CS, Fernandes LA, Silva ICB, Sampaio RA, Frazão LA. Phosphorus availability from natural and soluble phosphate sources for irrigated corn production. *African Journal of Agricultural Research*. 2015;10(32):3101-3106.

46. Velu S, Ramkumar V, Narayanan A, Swamy CS. Effect of interlayer anions on the physicochemical properties of zinc-aluminium hydrotalcite-like compounds. *Journal of Materials Science*. 1997;32(4):957-964.

47. Ferreira OP, Alves OL, Gouveia DX, Souza Filho AG, De Paiva JAC, Mendes Filho J. Thermal decomposition and structural reconstruction effect on Mg-Fe-based hydrotalcite compounds. *Journal of Solid State Chemistry*. 2004;177(9):3058-3069.

48. Marangoni R, Bouhent M, Taviot-Guého C, Wypych F, Leroux F. Zn2Al layered double hydroxides intercalated and adsorbed with anionic blue dyes: A physico-chemical characterization. *Journal of Colloid and Interface Science*. 2009;333(1):120-127.

49. Miyata S. Anion-Exchange Properties of Hydrotalcite-Like Compounds. *Clays and Clay Minerals*. 1983;31(4):305-311.

50. Millange F, Walton RI, Lei L, O'Hare D. Efficient Separation of Terephthalate and Phthalate Anions by Selective Ion-Exchange Intercalation in the Layered Double Hydroxide $Ca_2Al(OH)_6 \cdot NO_3 \cdot 2H_2O$. *Chemistry of Materials*. 2000;12(7):1990-1994.

51. Yang QZ, Sun DJ, Zhang CG, Wang XJ, Zhao WA. Synthesis and Characterization of Polyoxyethylene Sulfate Intercalated Mg-Al-Nitrate Layered Double Hydroxide. *Langmuir*. 2003;19(14):5570-5574.

52. Cantrell DG, Gillie LJ, Lee AF, Wilson K. Structure-reactivity correlations in MgAl hydrotalcite catalysts for biodiesel synthesis. *Applied Catalysis A: General*. 2005;287(2):183-190.

53. Costantino U, Marmottini F, Nocchetti M, Vivani R. New Synthetic Routes to Hydrotalcite-Like Compounds - Characterisation and Properties of the Obtained Materials. *European Journal of Inorganic Chemistry*. 1998;10:1439-1446.

54. Ookubo A, Ooi K, Tani F, Hayashi H. Phase Transition of Cl-Intercalated Hydrotalcite-like Compound during Ion Exchange with Phosphates. *Langmuir*. 1994;10(2):407-411.

55. Frost RL, Musumeci AW, Kloprogge JT, Adebajo MO, Martens WN. Raman spectroscopy of hydrotalcites with phosphate in the interlayer: implications for the removal of phosphate from water. *Journal of Raman Spectroscopy*. 2006;37(7):733-741.

56. Frost RL, Musumeci AW, Adebajo MO, Martens W. Using thermally activated hydrotalcite for the uptake of phosphate from aqueous media. *Journal Thermal of Analysis and Calorimetry*. 2007;89(1):95-99.

57. Arizaga GGC, Satyanarayana KG, Wypych F. Layered hydroxide salts: Synthesis, properties and potential applications. *Solid State Ionics*. 2007;178(15-18):1143-1162.

58. Yang K, Yan LG, Yang YM, Yu SJ, Shan RR, Yu HQ, et al. Adsorptive removal of phosphate by Mg-Al and Zn-Al layered double hydroxides: Kinetics, isotherms and mechanisms. *Separation and Purification Technology*. 2014;124:36-42.

59. Davydov AA. *Infrared Spectroscopy of Adsorbed Species on the Surface of Transition Metal Oxides*. New York: Wiley; 1990.

60. Hadjiivanov KI. Identification of Neutral and Charged Nx Oy Surface Species by IR Spectroscopy. *Catalysis Reviews*. 2000;42(1-2):71-144.

61. Prinetto F, Ghiotti G, Nova I, Lietti L, Tronconi E, Forzatti P. FT-IR and TPD Investigation of the NOx Storage Properties of BaO/Al_2O_3 and Pt-BaO/Al_2O_3 Catalysts. *The Journal Physical Chemistry B*. 2001;105(51):12732-12745.

62. Sedlmair C, Seshan K, Jentys A, Lercher JA. Elementary steps of NOx adsorption and surface reaction on a commercial storage-reduction catalyst. *Journal of Catalysis*. 2003;214(2):308-316.

63. da Silva V. *Potenciais Fertilizantes de Liberação Lenta de Nitrato Baseados em Hidróxidos Duplos Lamelares: Síntese, Caracterização e Propriedades*. [Thesis]. Curitiba: Federal University of Paraná; 2012.

64. Kloprogge JT, Hickey L, Frost RL. FT-Raman and FT-IR spectroscopic study of synthetic Mg/Zn/Al-hydrotalcites. *Journal of Raman Spectroscopy*. 2004;35(11):967-974.

65. Kloprogge JT. Infrared and Raman Spectroscopy of Naturally Occurring Hydrotalcites and Their Synthetic Equivalents. In: Kloprogge JT. *The Application of Vibrational Spectroscopy to Clay Minerals and Layered Double Hydroxides. Volume 13*. Chantilly: The Clay Minerals Society; 2005. p. 203-238.

66. Burrueco MI, Mora M, Jiménez-Sanchidrián C, Ruiz JR. Raman microspectroscopy of hydrotalcite-like compounds modified with sulphate and sulphonate organic anions. *Journal of Molecular Structure*. 2013;1034:38-42.

67. Wu PX, Li W, Zhu YJ, Tang YN, Zhu NW, Guo CL. The protective effect of layered double hydroxide against damage to DNA induced by heavy metals. *Applied Clay Science*. 2014;100:76-83.

68. Dobrea ID, Ciocan CE, Dumitriu E, Popa MI, Petit E, Hulea V. Raman spectroscopy - Useful tool for studying the catalysts derived from Mo and V-oxyanion-intercalated layered double hydroxides. *Applied Clay Science*. 2015;104:205-210.

69. Miranda LDL, Bellato CR, Milagres JL, Moura LG, Mounteer AH, de Almeida MF. Hydrotalcite-TiO_2 magnetic iron oxide intercalated with the anionic surfactant dodecylsulfate in the photocatalytic degradation of methylene blue dye. *Journal Environmental Management*. 2015;156:225-235.

70. Palmer SJ, Soisonard A, Frost RL. Determination of the mechanism(s) for the inclusion of arsenate, vanadate, or molybdate anions into hydrotalcites with variable cationic ratio. *Journal of Colloid and Interface Science*. 2009;329(2):404-409.

71. Kooli F, Rives V, Ulibarri MA. Preparation and Study of Decavanadate-Pillared Hydrotalcite-like Anionic Clays Containing Transition Metal Cations in the Layers. 1. Samples Containing Nickel-Aluminum Prepared by Anionic Exchange and Reconstruction. *Inorganic Chemistry*. 1995;34(21):5114-5121.

72. Lopez T, Bosch P, Ramos E, Gomez R, Novaro O, Acosta D, et al. Synthesis and Characterization of Sol-Gel Hydrotalcites. Structure and Texture. *Langmuir*. 1996;12(1):189-192.

73. Jaynes WF, Vance GF. BTEX Sorption by Organo-Clays: Cosorptive Enhancement and Equivalence of Interlayer Complexes. *Soil Science Society of America Journal*. 1996;60(6):1742-1749.

74. Di Cosimo JI, Di´ez VK, Xu M, Iglesia E, Apesteguí´a CR. Structure and Surface and Catalytic Properties of Mg-Al Basic Oxides. *Journal of Catalysis*. 1998;178(2):499-510.

75. You Y, Zhao H, Vance GF. Surfactant-enhanced adsorption of organic compounds by layered double hydroxides. *Colloids Surfaces A: Physicochemical and Engineering Aspects*. 2002;205(3):161-172.

76. Sing KSW. Reporting physisorption data for gas/solid systems with special reference to the determination of surface area and porosity (Recommendations 1984). *Pure and Applied Chemistry*. 1985;57(4):603-619.

77. Olson LM, Stroup WW, Paparozzi ET, Conley ME. *Model building in multi-factor plant nutrition experiments*. In: Proceedings of the 13th Conference on Applied Statistics in Agriculture; 2001; Manhattan, KS, USA. p. 183-206.

78. Cheng X, Huang X, Wang X, Sun D. Influence of calcination on the adsorptive removal of phosphate by Zn-Al layered double hydroxides from excess sludge liquor. *Journal of Hazardous Materials*. 2010;177(1-3):516-523.

79. Cheng X, Ye J, Sun D, Chen A. Influence of Synthesis Temperature on Phosphate Adsorption by Zn-Al Layered Double Hydroxides in Excess Sludge Liquor. *Chinese Journal of Chemical Engineering*. 2011;19(3):391-396.

80. Koilraj P, Antonyraj CA, Gupta V, Reddy CRK, Kannan S. Novel approach for selective phosphate removal using colloidal layered double hydroxide nanosheets and use of residue as fertilizer. *Applied Clay Science*. 2013;86:111-118.

81. Drenkova-Tuhtan A, Mandel K, Paulus A, Meyer C, Hutter F, Gellermann C, et al. Phosphate recovery from wastewater using engineered superparamagnetic particles modified with layered double hydroxide ion exchangers. *Water Research*. 2013;47(15):5670-5677.